Theory of the bound state between phonons and a CEF excitation in $CeAl_2$

J. Phys. C: Solid State Phys., 17 (1984) 4153–4177. Printed in Great Britain

Theory of the bound state between phonons and a CEF excitation in $CeAl_2$

P Thalmeier
Max-Planck-Institut für Festköperforschung, 7000 Stuttgart 80, Federal Republic of Germany

Received 31 October 1983, in final form 26 January 1984

Abstract. The coupling of lattice vibrations to the crystalline electric field (CEF) states of 4f electrons plays an important role in rare-earth compounds. It is shown that under favourable conditions this magnetoelastic interaction can lead to a 'bound state' between CEF excitations and lattice vibrations. The existence of this bound state in the intermetallic Laves phase $CeAl_2$ explains the results of inelastic neutron scattering investigations which have not been understood before. In this compound, a Γ_7–Γ_8 CEF excitation and low-lying vibrational modes of the Ce sublattice are involved in bound-state formation. The properties of this new type of excitation and its consequences for thermodynamic quantities are investigated. In addition the phonon softening at low temperatures found in $CeAl_2$ is discussed.

1. Introduction

In rare-earth (RE) compounds with a stable valence shell the ground-state multiplet with total angular momentum J is split into a series of crystalline electric field (CEF) states due to the electric field of the surrounding ions. The splitting of these states is generally of the order of 100 K so that they can be thermally populated. This leads to interesting temperature anomalies for many physical properties, notably the thermodynamic quantities and, for metallic CEF systems, also in the electronic transport coefficients. (For a review, see Fulde and Peschel 1972.) In addition the elastic (ultrasonic) properties are also strongly influenced at low temperatures (Lüthi 1980, Fulde 1978, Gehring and Gehring 1975) as seen in numerous RE compounds. This is due to the magnetoelastic coupling mechanism, i.e. the strain-induced change in the CEF potential. This mechanism is also important for high-frequency phonons, not only at ultrasonic frequencies. This has been shown in a series of Raman scattering experiments in the RE halogenides (Schaack 1977, Ahrens 1980) where optical phonons are strongly influenced by the coupling to CEF states. This kind of phenomena can also be investigated by inelastic neutron scattering experiments, which give information about the phonon dispersion as well as the position of the CEF levels. The latter can usually be classified according to the site symmetry of the RE ion. It was therefore a great surprise that this classification scheme did not work for $CeAl_2$ which showed a CEF excitation spectrum not compatible with the tetrahedral site symmetry of Ce. Furthermore, in later experiments strong temperature anomalies in the $CeAl_2$ phonon branches were observed. It is the aim of this paper to show that these effects are due to an extraordinarily strong magnetoelastic

0022-3719/84/234153 + 25 $02.25

coupling in $CeAl_2$ which leads to the formation of a bound state between low-lying phonons and a CEF excitation.

In § 2 the necessary experimental facts about $CeAl_2$ are discussed. In § 3 the principle of magnetoelastic interaction is explained and applied to $CeAl_2$. In the main part of § 3 it is shown how this interaction can lead to a CEF–phonon bound state and to a strong phonon renormalisation. In addition § 4 investigates the consequences for thermodynamic quantities and § 5 gives the conclusions.

2. Physical properties of $CeAl_2$

The intermetallic Laves phase $CeAl_2$ (figure 1) shows a remarkable variety of anomalous properties. At low temperatures this compound shows coexistence of Kondo lattice

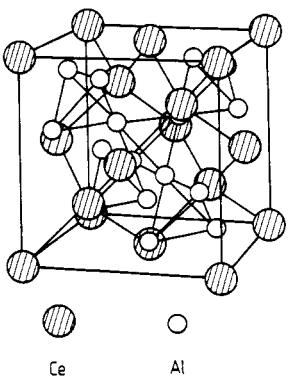

Figure 1. Conventional cubic unit cell of MAl_2 (M = RE). The RE ions form a diamond-type sublattice. The Al ions are placed on tetrahedrons. Lattice constant $a = 8.062$ Å for $CeAl_2$.

behaviour (Steglich *et al* 1979) with a Kondo temperature of $T_K \simeq 6$ K and antiferromagnetic ordering (Barbara *et al* 1979) at $T_N = 3.8$ K. The Ce ions are in a stable 3+ valence state with total angular momentum $J = \frac{5}{2}$. Because of the tetrahedral site symmetry this sixfold degenerate state should be split into a Γ_7 doublet and Γ_8 quartet by the crystalline electric field (CEF) of neighbouring ions. The Γ_7 ground state has a single-ion magnetic moment of 0.71 μ_B/site whose exchange interaction with conduction electrons leads to typical Kondo lattice type anomalies in electronic properties.

(i) A very high γ value ($\gamma_{CeAl_2} = 130\ \text{mJ K}^{-2}\text{mol}^{-1}$) in the specific heat compared with $LaAl_2$ where $\gamma_{LaAl_2} = 3.45\ \text{mJ K}^{-2}\text{mol}^{-1}$ (Steglich *et al* 1979). This is attributed to strong mass enhancement of conduction electrons by sf scattering.

(ii) Anomalies in the thermal expansion (Schefzyk *et al* 1983), magnetic susceptibility (Aarts 1983) and thermopower (Bauer *et al* 1982) which also suggest a Kondo effect.

In $CeAl_2$ the (negative) exchange interaction is not strong enough to screen out the 4f moments completely at low temperatures. Therefore the effective RKKY interaction between 4f moments leads to an incommensurate antiferromagnetic ordering at $T_N = 3.8$ K and consequently $CeAl_2$ is one of the few compounds which shows a coexistence of the Kondo effect and magnetic ordering (Jullien *et al* 1979). The magnetic ordering itself leads to additional anomalies in the electronic properties around T_N. Apart from its peculiar electronic properties, $CeAl_2$ has very abnormal lattice properties and, in

addition, a unique magnetic CEF excitation spectrum. This was found as a result of ultrasonic measurements (Godet and Purwins 1977, Lüthi and Lingner 1979, Penney *et al* 1982) and inelastic neutron scattering experiments (Loewenhaupt *et al* 1979 (LRS), Parks *et al* 1979, Reichardt 1983). Measurement of the elastic constants showed a pronounced softening of the c_{44} elastic constant at low temperatures which is due to a strong magnetoelastic coupling of transverse strain components to the CEF states of Ce^{3+} ions. From the temperature behaviour of c_{44}, a CEF splitting $\Gamma_7(0)$–$\Gamma_8(\Delta)$ of $\Delta \simeq 100$ K was deduced for the Ce^{3+} 4f states (Lüthi and Lingner 1979). However, inelastic neutron scattering (LRS) revealed a striking anomaly: instead of a single $\Gamma_7 \rightarrow \Gamma_8$ transition in the magnetic cross section *two* clearly separated peaks at about $\Delta_2 = 100$ K and $\Delta_1 = 180$ K (see figure 2(*a*)) have been observed. Somewhat larger values have been found

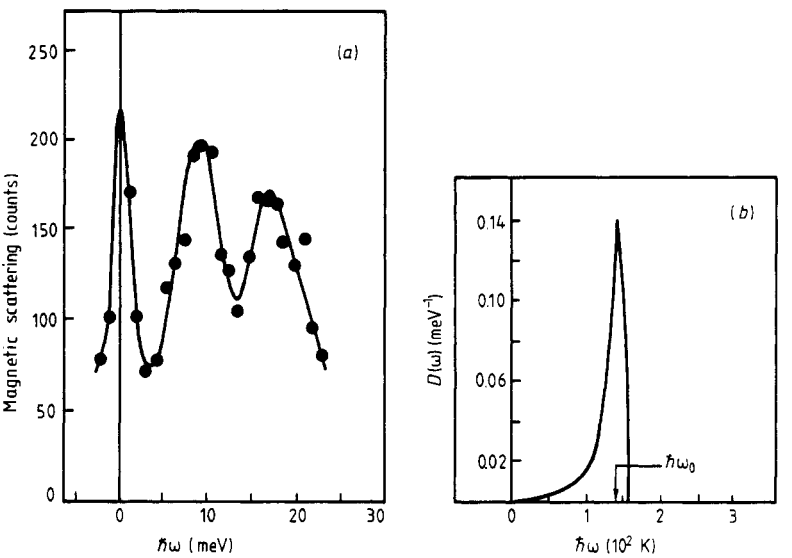

Figure 2. (*a*) Magnetic scattering rate as a function of energy transfer at $T = 60$ K (from LRS). (*b*) Phonon density of states (PDOS) corresponding to the six lowest LA, TA and LO, TO branches at $T = 296$ K (from Reichardt 1983). In the dispersionless model this is replaced by a single mode with $\hbar\omega_0 = 140$ K. In the triangular model for the PDOS the acoustic tail is neglected.

by Reichardt (1983): $\Delta_2 = 107$ K, $\Delta_1 = 200$ K. This seems to contradict the fact that the tetrahedral site symmetry of Ce^{3+} should lead to a cubic CEF which splits the $J = \frac{5}{2}$ ground state into a Γ_7 doublet and a Γ_8 quartet and consequently only *one* inelastic CEF transition should be observed. This cannot be caused by a static Jahn–Teller splitting of Γ_8 into two doublets; in this case it would be accompanied by a static lattice distortion. This has been ruled out by x-ray diffraction experiments (Steglich *et al* 1979) which show that $CeAl_2$ is cubic to within an accuracy of $\Delta a/a \simeq 10^{-5}$. Some clues to the origin of this anomalous magnetic excitation spectrum are given by the following experimental facts:

(i) Apparently both inelastic transitions must originate from a conventional $\Gamma_7 \rightarrow \Gamma_8$ excitation. This follows (LRS) from the determination of the ratio I_{in}/I_{el} where $I_{in} = I_{in}^{(1)} + I_{in}^{(2)}$ is the total inelastic intensity and I_{el} the intensity of quasielastic scattering which is entirely of Γ_7 origin at low temperatures ($T \simeq 5$ K). The experimental value $I_{in}/I_{el} = 3.2$ agrees with the expected value $\frac{16}{5}$ for the intensity ratio $I(\Gamma_7 \rightarrow \Gamma_8)/I(\Gamma_7 \rightarrow \Gamma_7)$ for normal Γ_7, Γ_8 CEF states.

(ii) The position of inelastic peaks and their splitting depends only weakly on the momentum transfer $\boldsymbol{Q}$ of neutrons, i.e. shows negligible dispersion.

(iii) The structure of the excitation spectrum does not change if $CeAl_2$ is diluted with La which has no f electrons (Horn 1983). Both peaks are observed in $La_{1-x}Ce_xAl_2$ down to a concentration of $x \simeq 0.07$ and do not change their position. A similar behaviour is observed for $Sc_{1-x}Ce_xAl_2$ (Horn 1983) down to $x \simeq 0.6$ where this alloy makes a transition to a mixed valence state so that both inelastic transitions merge into a broad quasi-elastic line whose width is characterised by the spin fluctuation time.

The latter two points suggest that one still observes localised excitations which can be understood within a single-ion picture. An attempt was made in LRS to explain the excitation spectrum by assuming a dynamical Jahn–Teller effect (DJTE) in the excited Γ_8 quartet. However, as the authors already noted one is forced to assume completely unphysical parameters for the DJTE model and therefore it has to be rejected.

It has been proposed that the anomalous magnetic excitation spectrum of $CeAl_2$ can be explained by the formation of a bound state between low-lying phonons and a Γ_7–Γ_8 CEF excitation (Thalmeier and Fulde 1982). In this paper I want to investigate the nature of this bound state in detail and consider its implications for some thermodynamic properties of $CeAl_2$. In addition I will discuss the strong temperature dependence of some phonon branches in $CeAl_2$ discovered recently (Reichardt 1983).

The neutron scattering investigations performed by Reichardt (1983) gave the first clue to the nature of the magnetic excitations found by LRS. He discovered that there are low-lying acoustic and optical phonon branches whose corresponding density of states peaks strongly around an energy $\hbar\omega_0 \simeq 140$ K (see figure 2(b)). (Phonon energies and CEF energies will be given in units of Kelvin i.e. $k_B \equiv 1$; 1 K = 0.086 meV, 1 meV = 11.605 K). These phonons correspond to motions of the heavy-diamond-type Ce sublattice (figure 1) alone. Phonons which include motions of the lighter Al atoms have energies greater than 230 K and will be neglected in all the following considerations. From figure 2 one can clearly see that the phonon peak lies just in between the two inelastic magnetic excitations at Δ_1 and Δ_2. At room temperature these phonons are hardly influenced by the coupling to the CEF excitations as will be explained later. Therefore, they should be very similar to the corresponding branches of the isomorphic $LaAl_2$ compound which has no 4f electrons. This has indeed been observed by Reichardt (1983) who also showed that a ten-parameter Born–von Karmán model can fit the experimental phonon dispersion quite well at room temperature. At this place it is instructive to recall some basic facts about neutron scattering. In RE compounds, magnetic scattering and phonon scattering compete with each other. The two contributions to the coherent differential cross section are essentially given by

$$\left(\frac{\mathrm{d}^2\sigma}{\mathrm{d}\omega\,\mathrm{d}\Omega}\right)_{\text{magn.}} \sim F^2(\boldsymbol{Q}) \int_{-\infty}^{\infty} \exp(\mathrm{i}\omega t)\langle \boldsymbol{J}_\perp(t)\,\boldsymbol{J}_\perp(0)\rangle\,\mathrm{d}t$$

$$\left(\frac{\mathrm{d}^2\sigma}{\mathrm{d}\omega\,\mathrm{d}\Omega}\right)_{\text{phon.}} \sim \boldsymbol{Q}^2 \int_{-\infty}^{\infty} \exp(\mathrm{i}\omega t)\langle \boldsymbol{u}_\parallel(t)\,\boldsymbol{u}_\parallel(0)\rangle\,\mathrm{d}t. \tag{1}$$

Here $\boldsymbol{J}_\perp$ and $\boldsymbol{u}_\parallel$ are the components of the magnetic moment and lattice displacement field which are perpendicular or parallel to the momentum transfer $\boldsymbol{Q}$ respectively.

$F(\boldsymbol{Q})$ is the magnetic form factor of the 4f shell, which decreases rapidly for $\boldsymbol{Q}$ larger than a few reciprocal lattice vectors. Because the phonon contribution increases $\sim \boldsymbol{Q}^2$ it is possible to separate the magnetic and phonon parts of the scattering cross section by going either to very low or very high momentum transfer $\boldsymbol{Q}$. The wavevector of the excitation is given by $\boldsymbol{q} = \boldsymbol{Q} - \boldsymbol{K}$, with $\boldsymbol{K}$ the nearest reciprocal lattice vector.

The position of the phonon peak in figure 2(*b*) suggests that these phonons are responsible for the observed splitting in the magnetic spectrum. In the next section I will describe the low-lying phonons in $CeAl_2$ in more detail and characterise their magnetoelastic interaction with the CEF states. It will be shown that this provides the mechanism for the anomalous excitation spectrum of $CeAl_2$.

3. Theory of the magnetic excitation spectrum and phonon softening in $CeAl_2$

To find out how the magnetoelastic interaction can influence the magnetic excitation spectrum two approaches are possible. In a simplified model the phonon dispersion is neglected and the Hamiltonian is diagonalised in a finite subspace of zero- and one-phonon states. This approach was used previously (Thalmeier and Fulde 1982) to explain the essential properties of the inelastic scattering cross section observed by LRS. A short review of this dispersionless model will be given below. If phonon dispersion is not neglected one gains a deeper insight into the problem, especially the formation of bound states between phonons and CEF excitations. For this purpose a more formal many-body approach with Green function techniques will be used later. In addition this allows us to calculate the temperature dependence of the average phonon energy. To proceed in the way indicated here one first has to classify the phonons and their possible magnetoelastic interactions in $CeAl_2$.

3.1. A model for the interaction of phonons and CEF excitations in $CeAl_2$

The phonons of interest here are those corresponding to the vibrations of the diamond-type Ce sublattice. Because one has two Ce atoms in the unit cell there are three acoustic and three optical branches. This labelling is somewhat arbitrary because along the symmetry directions $\Delta[100]$ and $\Delta[111]$ the transverse modes TA, TO belong to the same representation Δ_5 and Λ_3, respectively, and therefore are of mixed acoustic and optical nature. This means that their eigenvectors depend explicitly on the force constants and are not determined by symmetry alone (see, for example, Lax 1974). A peculiar property of these phonon branches in $CeAl_2$ is the extremely small splitting of acoustic and optical branches at the zone boundary X(001) and L(111) points. Because the largest contributions to the phonon density of states (PDOS) come from these points, one observes a single sharp peak in the total PDOS of acoustic and optical modes (figure 2(*b*)). The 'magnetoelastic coupling' of these phonons to the 4f CEF states of Ce^{3+} is due to the distortion of the local environment of each Ce^{3+} caused by each phonon mode ($\boldsymbol{ks}$). The distortion can be decomposed into contributions which transform as irreducible representations of the tetrahedral point group symmetry. For example, at the Γ point the optical phonon has $\Gamma_{25'}$ symmetry which produces local distortions of pure $\Gamma_5(T_{2g})$ type. As mentioned before the relative splittings of all six modes at the zone boundary are very small, therefore it is a fair approximation to describe them as a pair of triply degenerate modes having essentially the same Γ_5-symmetry distortions as at the zone centre. In the present model it will therefore be assumed that the magnetoelastic coupling

has only a contribution from local Γ_5-type distortions. In any case the coupling strength of Γ_5 distortions should be far larger than coupling by other symmetry distortions. This was suggested by point-charge calculations (Cullen and Clark 1977) and for $CeAl_2$ it was confirmed by ultrasonic measurements (Godet and Purwins 1977, Lüthi and Lingner 1979).

The coupled system of lattice vibrations and CEF excitations is described by the Hamiltonian $H = H_0 + H_1$ where H_0 is the non-interacting part and H_1 the magneto-elastic interaction:

$$H_0 = \sum_{\alpha n} \varepsilon_\alpha |\Gamma_\alpha^n\rangle\langle\Gamma_\alpha^n| + \sum_{ks} \hbar\omega_{ks}(a_{ks}^+ a_{ks} + \tfrac{1}{2}). \tag{2}$$

The first part of H_0 describes the unperturbed CEF states of Ce^{3+}, i.e. the conventional Γ_7–Γ_8 system whose energies are given by $(\Gamma_7): \varepsilon_7 = 0; (\Gamma_8): \varepsilon_8 = \Delta$. Of course, Δ cannot be obtained directly from neutron scattering but only the strongly renormalised double-peak spectrum with energies Δ_1 and Δ_2. It is reasonable to assume that Δ is not much different from the average $\frac{1}{2}(\Delta_1 + \Delta_2) \simeq 140$–$150$ K. The explicit form of the CEF states $|\Gamma_\alpha^n\rangle$ (α = multiplet, n = degeneracy index) for Ce^{3+} is given in table 1. The second part of H_0 describes the six (s = TA, LA, TO, LO) phonon branches of $CeAl_2$. The unperturbed phonon energies $\hbar\omega_{ks}$ do not yet include the effects of coupling to CEF states and correspond to those measured at room temperature where the effects of magneto-elastic coupling are negligible because of almost equally populated CEF states.

With the help of Steven's operator equivalents the most important contribution to H_1 of Γ_5 type is given by

$$H_1 = -\sum_{l\tau} \sum_{ks\mu} g_0^\mu(\boldsymbol{ks}, \tau)(a_{ks} + a_{-ks}^+) O_\mu(\boldsymbol{R}_{l\tau}) \exp(-\mathrm{i}\boldsymbol{k}\cdot\boldsymbol{R}_{l\tau}). \tag{3}$$

Here $\{O_\mu, \mu = 1, 2, 3\}$ are quadrupolar operators for the CEF states at site $\boldsymbol{R}_{l\tau}$ (l = lattice point, $\tau = 1, 2$ = basis index) which transform like a triplet Γ_5 representation under the tetrahedral point group T_d. They are given by

$$O_1 = J_yJ_z + J_zJ_y \qquad O_2 = J_zJ_x + J_xJ_z \qquad O_3 = J_xJ_y + J_yJ_x. \tag{4}$$

The coupling constants $g_0^\mu(\boldsymbol{ks}\tau)$ determine how strongly each mode $(\boldsymbol{ks})$ couples to the CEF states via a local Γ_5^μ distortion at each lattice site $\boldsymbol{R}_{l\tau}$. In principle they could be calculated within a point-charge model, this is however very impractical for general $\boldsymbol{k}$ and an average coupling strength will be used later on. In the basis states of table 1 the quadrupolar operators are given by

$$O_2 = \left(\begin{array}{cccc|cc} 0 & 0 & -\alpha & 0 & -\beta & 0 \\ 0 & 0 & 0 & \alpha & -\gamma & 0 \\ -\alpha & 0 & 0 & 0 & 0 & \gamma \\ 0 & \alpha & 0 & 0 & 0 & \beta \\ \hline -\beta & -\gamma & 0 & 0 & 0 & 0 \\ 0 & 0 & \gamma & \beta & 0 & 0 \end{array}\right) \begin{array}{l} \left.\begin{array}{l}\\\\\\\end{array}\right\} \Gamma_8 \\ \left.\begin{array}{l}\\\end{array}\right\} \Gamma_7 \end{array} \tag{5}$$

$$\alpha = 1.1547, \beta = 4.4721, \gamma = 2.5820$$

O_1 and O_3 can be expressed in a similar way. This shows that phonons have a Γ_5-type coupling to $\Gamma_7 \rightarrow \Gamma_8$ and $\Gamma_8 \rightarrow \Gamma_8$ CEF transitions. Because Γ_7 is a Kramers doublet, time-reversal symmetry requires that all quadrupolar $\Gamma_7 \rightarrow \Gamma_7$ matrix elements vanish.

Table 1. The CEF states of Ce^{3+} in terms of $|J = \frac{5}{2}, M\rangle$ free-ion states $a = (\frac{1}{6})^{1/2}$; $b = (\frac{5}{6})^{1/2}$.

$\|\Gamma_8^1\rangle = b\|\frac{5}{2}\rangle + a\|-\frac{3}{2}\rangle$
$\|\Gamma_8^2\rangle = \|\frac{1}{2}\rangle$
$\|\Gamma_8^3\rangle = \|-\frac{1}{2}\rangle$
$\|\Gamma_8^4\rangle = b\|-\frac{5}{2}\rangle + a\|\frac{3}{2}\rangle$
$\|\Gamma_7^1\rangle = a\|-\frac{5}{2}\rangle - b\|\frac{3}{2}\rangle$
$\|\Gamma_7^2\rangle = -\|\frac{5}{2}\rangle - b\|-\frac{3}{2}\rangle$

A measure for the relative weight of these transitions is given by the oscillator strengths

$$Q_{\alpha\beta} = \sum_{n,m} |\langle\Gamma_\alpha^m|O_\mu|\Gamma_\beta^n\rangle|^2$$

which are independent of μ because of cubic symmetry. We have $Q_{78} = Q_{87} = 2(\beta^2 + \gamma^2) = 53.33$ and $Q_{88} = 4\alpha^2 = 5.33$. This shows that the phonon coupling to the inelastic $\Gamma_7 \leftrightarrow \Gamma_8$ transitions is most important.

3.2. The dispersionless model and the magnetic structure function

The dispersionless model is a reasonable first approximation considering the narrow phonon DOS in figure 2(*b*). In this model the six phonon branches ω_{ks} are replaced by a triply degenerate local oscillator of energy $\hbar\omega_0 = 140$ K which produces Γ_5-type strains at the Ce^{3+} sites. In this case there is no difference between 'acoustic' and 'optical' modes, furthermore T_d site symmetry requires $g_0^\mu = g_0$ for the coupling constants. The Hamiltonian is then given by

$$H = \sum_{\alpha n} \varepsilon_\alpha |\Gamma_\alpha^n\rangle\langle\Gamma_\alpha^n| + \hbar\omega_0 \sum_\mu (a_\mu^+ a_\mu + \tfrac{1}{2}) - g_0 \sum_\mu (a_\mu + a_\mu^-)\, O_\mu. \tag{6}$$

The eigenstates of H have been calculated within the twelve-dimensional subspace $\{|\psi_\kappa\rangle,\ \kappa = 1, \ldots, 12\}$ of zero- and one-phonon states $|\Gamma_\alpha^n, 0\rangle$ ($\alpha = 7, 8$) and $|\Gamma_7^n, \mu\rangle = a_\mu^+|\Gamma_7^n, 0\rangle$ with unperturbed energies $0, \Delta, \hbar\omega_0\ (\simeq\Delta)$ respectively (Thalmeier and Fulde 1982). They were shown to consist of two quartets $|\tilde\Gamma_{81}\rangle|\tilde\Gamma_{82}\rangle$ and two doublets $|\tilde\Gamma_6\rangle$, $|\tilde\Gamma_7\rangle$. Their energies are given by

$$\begin{aligned} &\tilde\varepsilon_{8(1,2)} = \tfrac{1}{2}(\Delta + \hbar\omega_0) \pm [\tfrac{1}{4}(\Delta - \hbar\omega_0)^2 + g_0^2\gamma_0^2]^{1/2} \\ &\tilde\varepsilon_6 = \hbar\omega_0 \qquad \tilde\varepsilon_7 = 0 \\ &\gamma_0^2 = \sum_{\mu,n} |\langle\Gamma_8^m|O_\mu|\Gamma_7^n\rangle|^2 = 40. \end{aligned} \tag{7}$$

The $|\tilde\Gamma_{8(1,2)}\rangle$ states are linear combinations of purely electronic $|\tilde\Gamma_8, 0\rangle$ states and one-phonon states $|\Gamma_7, \mu\rangle$. They can be interpreted as bound and anti-bound states of a CEF excitation and phonons as shown in § 3.3. The $|\tilde\Gamma_6\rangle$ state has phonon character and therefore its energy is independent of Δ. The $|\tilde\Gamma_7\rangle$ is the original electronic Kramers doublet. The energy levels (7) were plotted as a function of Δ in Thalmeier and Fulde (1982). The dipolar matrix elements

$$d_{\alpha\beta} = \sum_{n,m} |\langle\tilde\Gamma_\alpha^n|J_z|\tilde\Gamma_\beta^m\rangle|^2$$

determine which transitions contribute to the magnetic scattering. One finds $d_{76} \equiv 0$ and $d_{7,81} \simeq d_{7,82} = 2.2$ for $\Delta \simeq \hbar\omega_0$. This explains the existence of two inelastic peaks of about equal strength in a natural way. They correspond to the $\tilde\Gamma_7 \rightarrow \tilde\Gamma_{81}, \tilde\Gamma_{82}$ transitions

in the present model. Furthermore with $d_{77} = 1.39$ the rate of total inelastic-to-quasi-elastic scattering for $kT/\Delta \ll 1$ is given by $(d_{7,81} + d_{7,82})/d_{77} = 3.2$. This is equal to the experimental value and also corresponds to the value $\frac{16}{5}$ which one would expect for a conventional Γ_7–Γ_8 scheme.

The coupling constant g_0 is the only fitting parameter in the model and it has been chosen as $g_0 = 6.3$ K in order that $\tilde{\varepsilon}_{81}$ and $\tilde{\varepsilon}_{82}$ agree with the experimental peak positions Δ_1 and Δ_2 respectively. The size of g_0 will be discussed later on. In reality the inelastic magnetic excitations are broadened by the interaction with the conduction electrons of $CeAl_2$, which is assumed to be of exchange type:

$$H_{ex} = -I_{ex}(g - 1)\, s \cdot J. \tag{8}$$

Here I_{ex} is the exchange constant, g the Landé factor ($g_{Ce^{3+}} = \frac{6}{7}$) and s and J conduction electron spin and 4f total angular momentum respectively. The relaxation of ordinary CEF excitations due to H_{ex} has been discussed by Becker *et al* (1977) using the Zwanzig–Mori formalism. This approach is also adopted here for the CEF–phonon bound states. Using the fluctuation-dissipation theorem, the magnetic cross section in equation (1) is given by

$$\left(\frac{d^2\sigma}{d\omega\, d\Omega}\right)_{magn.} \sim F(Q)^2 S(\omega)$$

$$S(\omega) = [1 - \exp(-\beta\omega)]\, \mathrm{Im}\, u(\omega)$$

$$u(\omega) = \int_0^\infty \langle [J_z(t), J_z] \rangle \exp[i(\omega + i\eta)t]\, dt. \tag{9}$$

Here non-interacting RE ions have been assumed and therefore the spectral function $S(\omega)$ is determined by the dynamical single-ion susceptibility $u(\omega)$. In second-order perturbation theory, with respect to H_{ex}, one obtains (Becker *et al* 1977):

$$\mathrm{Im}\, u(\omega) = \omega \sum_{ij,i'j'} u_0(ij)\, \mathrm{Im}\, \Omega^{-1}_{ij,i'j'}(\omega)$$

where

$$u_0(ij) = |\langle i|J_z|j\rangle|^2 \times \begin{cases} \dfrac{p_j - p_i}{\tilde{\varepsilon}_j - \tilde{\varepsilon}_i} & \tilde{\varepsilon}_i \neq \tilde{\varepsilon}_j \\ \beta p_i & \tilde{\varepsilon}_i = \tilde{\varepsilon}_j \end{cases} \tag{10}$$

and

$$\Omega_{ij,i'j'}(\omega) = (\tilde{\varepsilon}_i - \tilde{\varepsilon}_j + \omega)\, \delta_{ij,i'j'} - i\Delta_{ij,i'j'}(\omega).$$

Here i, j denote any of the states $|\tilde{\Gamma}^n_a\rangle$, $\tilde{\varepsilon}_i$ their energies and $p_i = \exp(-\beta\tilde{\varepsilon}_i)/Z$ their thermal occupations, where Z is the partition function.

The memory function matrix $\boldsymbol{\Delta}$ leads to a damping of the various excitations described by the frequency matrix $\boldsymbol{\Omega}$. Using the explicit form of $\boldsymbol{\Delta}$ in second-order perturbation theory ($\sim I_{ex}^2$) the spectral function $S(\omega)$ has been computed. This is shown in figure 3 for two temperatures. According to (9) this function should be directly proportional to the cross section and the qualitative agreement with figure 2(a) is quite obvious. A quantitative comparison is not yet possible because figure 2(a) shows the raw scattering data which still includes the experimental resolution function. In figure 3 $S(\omega)$ has been plotted instead of $\tilde{S}(\omega) = S(\omega) + S(-\omega)$ as in Thalmeier and Fulde (1982); the frequency integral of $S(\omega)$ is not normalised to $2\pi\langle J_z^2\rangle$ as for $\tilde{S}(\omega)$.

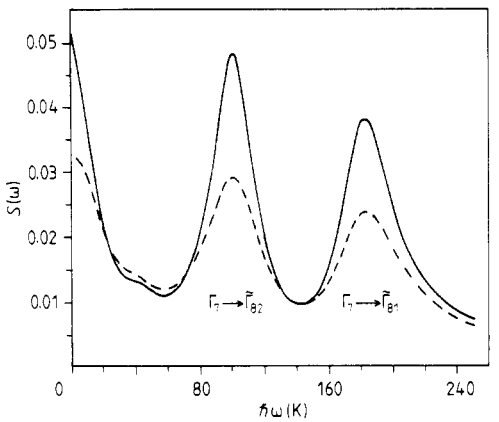

Figure 3. Magnetic structure function $S(\omega)$ in the dispersionless model. Broadening of transitions is due to exchange interaction with conduction electrons where $I_{ex}N(0) = 0.06$ is used. (I_{ex} is the exchange constant, $N(0)$ is the electron DOS at the Fermi level). Full curve, $T = 60$ K; broken curve, $T = 80$ K.

In figure 3 $\Delta = \hbar\omega_0 = 140$ K was assumed which means that $\bar{\Gamma}_7 \rightarrow \bar{\Gamma}_{8(1,2)}$ should have equal intensities because of $d_{7,81} = d_{7,82}$. In fact, due to coupling of all the inelastic and elastic transitions via the non-diagonal parts of the memory matrix $\boldsymbol{\Delta}(\omega)$, (10), the intensity is shifted to lower frequencies so that the height of the $\Gamma_7 \rightarrow \bar{\Gamma}_{81}$ peak is reduced. For high temperatures, $kT \gtrsim \Delta$, only a broad quasi-elastic line remains.

Finally I want to discuss whether the size of $g_0 = 6.3$ K as determined from the $\bar{\Gamma}_{81}$–$\bar{\Gamma}_{82}$ splitting is reasonable and make a comparison with other MAl_2 compounds (M = RE). A useful test is the comparison with the properly normalised coupling constants of c_{44} transverse sound modes. They produce local Γ_5-type distortions and therefore have the same magnetoelastic coupling mechanism as the $\hbar\omega_0$ phonons in the model discussed above. The coupling of long-wavelength phonons is usually described in the continuum approximation. For c_{44} modes one has:

$$H_{me}(c_{44}) = -g_3 \sum_l 2(\varepsilon_{yz}O_{yz} + \varepsilon_{xz}O_{xz} + \varepsilon_{xy}O_{xy}). \tag{11}$$

Here ε_{yz} etc are the transverse strain components and O_{yz}, O_{zx} and O_{xy} etc are the same as in (4).

For a sound wave with wavevector $\boldsymbol{k} \| \hat{\boldsymbol{z}}$ and polarisation $\boldsymbol{e} \| \hat{\boldsymbol{x}}$, the expansion of ε_{xz} in the phonon coordinates leads to

$$H_{me}(c_{44}) = -\sum_{lk} \tilde{g}_3(\boldsymbol{k})\, \varphi_{k\boldsymbol{e}} O_{xz}(l) \exp(\mathrm{i}\boldsymbol{k} \cdot \boldsymbol{R}_l) \tag{12}$$

where $|\tilde{g}_3|^2 = g_3^2(\hbar k^2/2MN\omega_k)$. A wavevector-independent measure of the coupling strength is then given by $\tilde{g}_3^2/\hbar\omega_k = g_3^2/Vc_{44}$ where V is the volume per Ce atom. This constant is determined by measuring the temperature dependence of the c_{44} elastic constant which is given by $c_{44}(T)/c_{44}(0) = [1 - (g_3^2/c_{44}V)u_Q(T)]$ where $u_Q(T)$ is the static quadrupolar susceptibility. This leads to $g_3^2/c_{44}V = 368$ mK (Lüthi and Lingner 1979). The Hamiltonian (12) is of the same form as the interaction part in (6), the wavevector-independent coupling strength $\tilde{g}_3^2(k)/\hbar\omega_k = g_3^2/Vc_{44}$ should be comparable with $g_0^2/\hbar\omega_0$. For $g_0 = 6.3$ K, as derived from the Δ_1–Δ_2 splitting and $\hbar\omega_0 = 140$ K this leads to $g_0^2/\hbar\omega_0 = 283$ mK, which agrees with g_3^2/Vc_{44} to within thirty per cent. This is strong evidence that the magnetoelastic coupling is responsible for both the elastic

constant anomaly and the peculiar magnetic excitation spectrum. The coupling strengths $(g_3^2/Vc_{44})^{1/2}$ have been measured for a whole series of MAl_2 components (M = RE) (Lingner and Lüthi (1983) and references cited therein). They are given in table 2. One can see that the coupling strength for $CeAl_2$ is larger by at least one order of magnitude compared with the other MAl_2. In a point-charge model (PCM) these constants can be computed and one obtains $g_3 = C_{\Gamma_5}\alpha_J\langle r^2\rangle_{4f}$ where C_{Γ_5} is a constant depending on the site coordination and strain type (Γ_5) and α_J and $\langle r^2\rangle_{4f}$ are the Stevens factor and mean-square radius which characterises the 4f ground state. Although the point-charge values for g_3 show a tendency to increase from $TmAl_2$ towards $CeAl_2$, the PCM is clearly unable

Table 2. The magnetoelastic coupling constants $(g_3^2/Vc_{44})^{1/2}$ are given for some MAl_2 compounds (M = RE) (from Lingner and Lüthi 1983). In the point-charge model they should be proportional to $\alpha_J\langle r^2\rangle_{4f}$. ($a_0$ is the Bohr radius). The coupling constants have been determined by ultrasonic experiments.

MAl_2	$(g_3^2/Vc_{44})^{1/2}$ ($mK^{1/2}$)	$\lvert\alpha_J\rvert\langle r^2\rangle_{4f}$ ($10^{-2}a_0^2$)
$CeAl_2$	19.07	6.86
$PrAl_2$	2.01	1.14
$NdAl_2$	1.08	0.64
$TmAl_2$	0.55	0.65

to explain the exceptionally large value of g_3 in $CeAl_2$. It is reasonable to assume that the origin of a large g_3 and equivalently g_0 lies in the hybridisation of the 4f electron shell in Ce^{3+} with conduction electrons. This mechanism is strong for many intermetallic Ce compounds because the weakly bound $4f^1$ state is closely below the Fermi energy. It is also known to be responsible for the anomalously large exchange interaction and resulting T_c reduction in the $La_{1-x}Ce_xAl_2$ compounds (Maple 1976).

In principle an arbitrary small coupling constant g_0 would lead to a splitting into $\tilde{\Gamma}_{81}$ and $\tilde{\Gamma}_{82}$ bound states in the dispersionless model which would be unobservable if it is smaller than the linewidth due to exchange scattering. This might explain why similar states have not been observed in other MAl_2 assuming the position of their CEF levels and phonon energies was not too unfavourable already. On the other hand, inclusion of phonon dispersion will show that even without taking extrinsic damping by conduction electrons into account, a minimum threshold value for the coupling strength g_0 is necessary to observe the splitting into $\tilde{\Gamma}_{81}$, $\tilde{\Gamma}_{82}$ states which justifies calling them 'bound states' of a CEF excitation and phonons.

3.3. Green functions and the CEF–phonon bound states

To gain more insight into the nature of the bound states it is necessary to consider the coupling of CEF excitations to a whole band of phonon states instead of a single oscillator mode with energy $\hbar\omega_0$. In analogy to the dispersionless model the eigenstates of the interacting systems could be written as superpositions of zero- and one-phonon states but with a summation over all phonons ($\boldsymbol{ks}$) included:

$$|\tilde{\Gamma}_\alpha^m\rangle_l = \sum_{ksn} u_{\alpha s}^{mn}(\boldsymbol{k})a_{\boldsymbol{ks}}^+|\Gamma_7^n\rangle_l + \sum_n v_\alpha^{mn}|\Gamma_8^n\rangle_l. \tag{13}$$

Here v and u are the zero- and one-phonon amplitudes of the eigenstate, respectively, $|\tilde{\Gamma}_\alpha^m\rangle_l$ where l is the site index. The eigenvalue equations are then integral equations for these amplitudes. Such an approach would be very similar to the one used in the theory of exciton–phonon bound states in semiconductors (Toyozawa and Hermanson 1968) except that excitonic transitions are replaced by CEF transitions. In the present problem, however, it is better to adopt a more formal many-body approach which can be more directly interpreted in terms of physical processes. For this purpose the temperature Green functions for phonons and CEF states are needed. Their Fourier transforms are given by

$$D_0(\boldsymbol{ks}, \omega_m) = 2\omega_{ks}/[(\mathrm{i}\omega_m)^2 - \omega_{ks}^2] \qquad \omega_m = 2m\pi T$$
$$G_0(l, i, \omega_n) = [\mathrm{i}\omega_n - (\varepsilon_i + \lambda(l))]^{-1} \qquad \omega_n = (2n+1)\pi T \tag{14}$$

for phonons and CEF excitations respectively. The Abrikosov pseudo-fermion technique is used which represents CEF states $|i\rangle$ with energy ε_i with fermion Green functions that have an adjustable chemical potential $\lambda(l)$ (l = site index). Although this representation introduces unphysical states they have no effects if at the end of the calculation a proper limit $\lambda(l) \to \infty$ is taken. For a detailed description of this technique see Fulde and Peschel (1972). In this pseudo-fermion basis the Hamiltonian is (cf (2), (3))

$$H_0 = \sum_{i,l} (\varepsilon_i + \lambda(l)) c_i^\dagger(l) c_i(l) + \sum_{ks} \omega_{ks}(a_{ks}^\dagger a_{ks} + \tfrac{1}{2})$$
$$H_1 = -\sum_{k,\mu,l} g_k^\mu O_{ij}^\mu (a_k + a_{-k}^\dagger) c_i^\dagger(l) c_i(l) \exp(\mathrm{i}\boldsymbol{k} \cdot \boldsymbol{R}_l). \tag{15}$$

The $c_i^\dagger$ are the pseudo-fermion operators for the CEF states $|i\rangle$ and their non-interacting Green function is given by G_0. The basis index τ and polarisation index s have been suppressed in H_1. The interacting CEF–phonon system is described by the Dyson equations for the renormalised CEF and phonon Green functions and the usual diagrammatic methods can be applied. The Dyson equations in the RPA approximation for the self-energies are shown in figure 4.

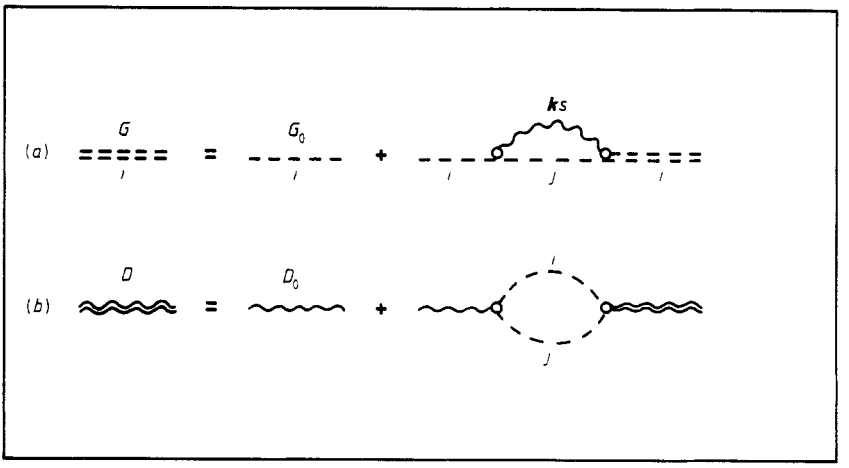

Figure 4. Diagrammatic Dyson equations in RPA for the Green functions of CEF states (G_0, G: broken lines) and phonon s (D_0, D: wavy lines). Single lines correspond to the bare G_0, D_0 and double lines to the renormalised G, D.

3.3.1. The CEF–self-energy and the existence of a bound state. The renormalised CEF pseudo-fermion propagator is given by

$$G = (G_0^{-1} - \Sigma_c)^{-1}$$

$$G(l, i, \omega_n) = \left(i\omega_n - \lambda(l) - \varepsilon_i - \Sigma_c(l, i, \omega_n)\right)^{-1}. \tag{16}$$

Σ_c is the self-energy of a CEF–pseudo-fermion state $|i\rangle$ due to the virtual excitation of intermediate phonons of arbitrary $(\boldsymbol{k}s)$ (figure 4(a)) and a simultaneous virtual CEF transition $|i\rangle \leftrightarrow |j\rangle$. This virtual excitation of a phonon cloud happens at a given site l, intersite processes do not contribute to Σ_c in the RPA of figure 4(a). Explicitly, Σ_c is given by

$$\Sigma_c(i, \omega_n) = -\beta^{-1} \sum_{\omega_{n'} k\mu j} |g_k^\mu|^2 |O_{ij}^\mu|^2 G_0(l, j, \omega_{n'}) D_0(\boldsymbol{k}, (\omega_n - \omega_{n'})). \tag{17}$$

Summation over Matsubara frequencies results in

$$\Sigma_c(i, \omega_n) = \sum_{k\mu j} |g_{k\mu}|^2 |O_{ij}^\mu|^2 \left(\frac{1 + n(\omega_k)}{i\omega_n - \varepsilon_j - \lambda - \omega_k} + \frac{n(\omega_k)}{i\omega_n - \varepsilon_j - \lambda + \omega_k}\right). \tag{18}$$

Here $n(\omega_k) = [\exp(\beta\omega_k) - 1]^{-1}$ is the Bose factor and the first and second terms in (18) correspond to virtual-phonon emission and absorption respectively. As long as kT is appreciably smaller than the average phonon frequency $\hbar\omega_0$, $n(\omega_k) \simeq 0$ and only the first term is important. After analytic continuation and with the definitions

$$\tilde{G}(i, \omega) = G(i, \omega + \lambda) \quad \tilde{\Sigma}_c(i, \omega) = \Sigma_c(i, \omega + \lambda) \tag{19}$$

one obtains

$$\tilde{\Sigma}_c(i, \omega) = \sum_{k\mu j} \frac{|g_{k\mu}|^2 |O_{ij}^\mu|^2}{\omega - \varepsilon_i - \omega_k + i\eta}$$

$$\tilde{G}(i, \omega) = \left(\omega - \varepsilon_i - \tilde{\Sigma}_c(i, \omega) + i\eta\right)^{-1}. \tag{20}$$

Without coupling $\tilde{\Sigma}_c = 0$ and $\tilde{G}$ has poles at the undisturbed CEF energies ε_i ($\varepsilon_{\Gamma_7} = 0$, $\varepsilon_8 = \Delta$), i.e. its spectral function $S_c(i, \omega) = -\pi^{-1} \operatorname{Im} \tilde{G}(i, \omega)$ is a δ-function at ε_i. It will now be discussed how a non-zero magnetoelastic self-energy Σ_c changes the spectral function of the propagators $\tilde{G}(i, \omega)$. For this purpose two approximations will be made to calculate $\tilde{\Sigma}_c(i, \omega)$:

(i) $g_k^\mu \equiv g_0$ is independent of $\boldsymbol{k}$, μ; in this case the $\boldsymbol{k}$-summation in (20) can be changed to an integration over the phonon density of states.

(ii) The phonon density of states (PDOS) is described by a triangular DOS function normalised to unity: $(\omega_b = \omega_2 - \omega_1)$

$$D(\omega) = \begin{cases} (2/\omega_b)^2(\omega - \omega_1) & \omega_1 < \omega < \omega_0 \\ (2/\omega_b)^2(\omega_2 - \omega) & \omega_0 < \omega < \omega_2 \\ 0 & \text{elsewhere.} \end{cases} \tag{21}$$

Here the minimum, average and maximum energies are given by $\hbar\omega_1 = 120$ K, $\hbar\omega_0 = 140$ K and $\hbar\omega_2 = 160$ K respectively. The real PDOS of figure 2(b) is simulated rather well by $D(\omega)$. Here $\hbar\omega_0$ is the average unrenormalised phonon energy at high (room) temperatures.

With the approximations described before one obtains

$$\tilde{\Sigma}_c(i,\omega) = g_0^2 \sum_j \left(\sum_\mu |O_{ij}^\mu|^2 \right) H(\omega - \varepsilon_j) = \tilde{\Sigma}_1(i,\omega) + i\tilde{\Sigma}_2(i,\omega)$$

$$H(\omega) = H_1(\omega) + i H_2(\omega) = P \int \frac{D(\omega')}{\omega - \omega'} d\omega' - i\pi D(\omega). \tag{22}$$

The real part $H_1(\omega)$ can be obtained by a simple integration:

$$H_1(\omega) = \left(\frac{2}{\omega_b}\right)^2 \left((\omega_1 - \omega) \ln \left| \frac{\omega - \omega_0}{\omega - \omega_1} \right| + (\omega_2 - \omega) \ln \left| \frac{\omega - \omega_0}{\omega - \omega_2} \right| \right). \tag{23}$$

This function is antisymmetric with respect to $\omega = \omega_0$; it is shown in figure 5(*a*). The inflection points are at $\omega = \omega_{1,2}$ with $|f(\omega_{1,2})| = 4 \ln 2/\omega_b$.

With the knowledge of $\tilde{\Sigma}_c(i,\omega)$ one can discuss the spectral properties of $\tilde{G}(i,\omega)$ for several interesting cases. Explicitly, the self-energies for Γ_7 and Γ_8 are given by

$$g_0^{-2}\tilde{\Sigma}_c(\Gamma_8,\omega) = \gamma_0^2 H_1(\omega) + \gamma_1^2 H_1(\omega - \Delta) - i\pi(\gamma_0^2 D(\omega) + \gamma_1^2 D(\omega - \Delta))$$

$$g_0^{-2}\tilde{\Sigma}_c(\Gamma_7,\omega) = \gamma_0^2 H_1(\omega - \Delta) - i\pi\gamma_1^2 D(\omega - \Delta). \tag{24}$$

Here

$$\gamma_0^2 = \sum_{\mu m} |\langle \Gamma_8^n | O_\mu | \Gamma_7^m \rangle|^2 = 40 \qquad \gamma_1^2 = \sum_{\mu m} |\langle \Gamma_8^n | O_\mu | \Gamma_8^m \rangle|^2 = 4$$

where n denotes any of the Γ_8 states. The spectral function is given by

$$S_c(i,\omega) = -\frac{1}{\pi} \operatorname{Im} \tilde{G}(i,\omega)$$

$$= \frac{-\pi^{-1}(\tilde{\Sigma}_2(i,\omega) + \eta)}{(\omega - \varepsilon_i - \tilde{\Sigma}_1(i,\omega))^2 + (\tilde{\Sigma}_2(i,\omega)^2 + \eta^2}. \tag{25}$$

Again for $\tilde{\Sigma}_c \equiv 0$, this describes a δ-function at $\omega = \varepsilon_i$. For non-zero $\tilde{\Sigma}_c$, $S_c(i,\omega)$ can exhibit two features:

(i) If ω is in a region where $\tilde{\Sigma}_2(i,\omega) \neq 0$, $S_c(i,\omega)$ is a smooth function which describes the possible decay of the CEF state $|i\rangle$ into the phonon continuum.

(ii) In regions where $\tilde{\Sigma}_2(i,\omega) = 0$, $S_c(i,\omega)$ may have δ-function contributions whose positions are given by the solutions of

$$\omega - \varepsilon_i - \tilde{\Sigma}_1(i,\omega) = 0. \tag{26}$$

If $\tilde{\Sigma}_1$ is small, they correspond to the original δ-peaks at ε_i shifted by a small energy. If $\tilde{\Sigma}_1$ is large, one has a qualitatively new situation with new δ-peaks occurring far away from the original peak at the undisturbed ε_i. With (24) this can be studied in detail. The terms of the order of γ_1^2 in the Γ_8 self-energy are due to virtual $\Gamma_8 \leftrightarrow \Gamma_8$ scattering. For the interesting region $\hbar\omega \simeq \Delta, \hbar\omega_0$ one can write

$$g_0^{-2}\tilde{\Sigma}(\Gamma_8,\omega) \simeq \gamma_0^2 H_1(\omega) + \gamma_1^2 H_1(0) - i\pi\gamma_0^2 D(\omega). \tag{27}$$

Inserting this into (25) one obtains ($\lim_{\eta \to 0}$ implied)

$$S_c(\Gamma_8,\omega) = \frac{g_0^2\gamma_0^2 D(\omega) + \eta}{(\omega - \Delta' - g_0^2\gamma_0^2 H_1(\omega))^2 + (g_0^2\gamma_0^2 D(\omega))^2 + \eta^2} \tag{28}$$

where $\Delta' = \Delta + \gamma_1^2 H_1(0)$ is the Γ_8-energy renormalised by diagonal $\Gamma_8 \leftrightarrow \Gamma_8$ scattering. This correction is small and $\Delta' \simeq \Delta$ can be assumed. For the Γ_7 Green function around $\omega \simeq 0$ only non-resonant self-energy terms contribute to (24):

$$\tilde{\Sigma}(\Gamma_7, \omega) \simeq g_0^2 \gamma_0^2 H_1(-\Delta). \tag{29}$$

Therefore the corresponding function will again be a δ-function shifted from $\varepsilon_7 = 0$ by the amount given in (29) which is small and will therefore be neglected. Consequently the Γ_7 propagator is essentially unchanged by the process shown in figure 4(*a*):

$$\tilde{G}(\Gamma_7, \omega) \simeq 1/(\omega + i\eta). \tag{29a}$$

The more interesting case is the Γ_8-spectral function (28) which includes the resonant contributions of Γ_7–Γ_8 virtual excitations. Three different situations may occur corresponding to the possible solutions of (26) and the behaviour of (25). For $i = \Gamma_8$ (26) leads to

$$\alpha^{-2}(\omega - \Delta) = H_1(\omega) \qquad \alpha^2 = g_0^2 \gamma_0^2. \tag{30}$$

These solutions can be found graphically as shown in figure 5.

(i) If α^2 is small and Δ is outside $[\omega_1, \omega_2]$, only one solution exists, whose energy is approximately given by $\Delta' \simeq \Delta + \alpha^2 H_1(\Delta)$ and which describes the position of a δ-contribution to $S_c(\Gamma_8, \omega)$.

(ii) For α^2 small but Δ inside $[\omega_1, \omega_2]$, the δ-function is broadened into a Lorentzian with centre $\Delta' = \Delta + \alpha^2 H(\Delta)$ and width $\Gamma \simeq \alpha^2 D(\Delta')$, describing the possible decay of the Γ_8 excitation into the phonon continuum.

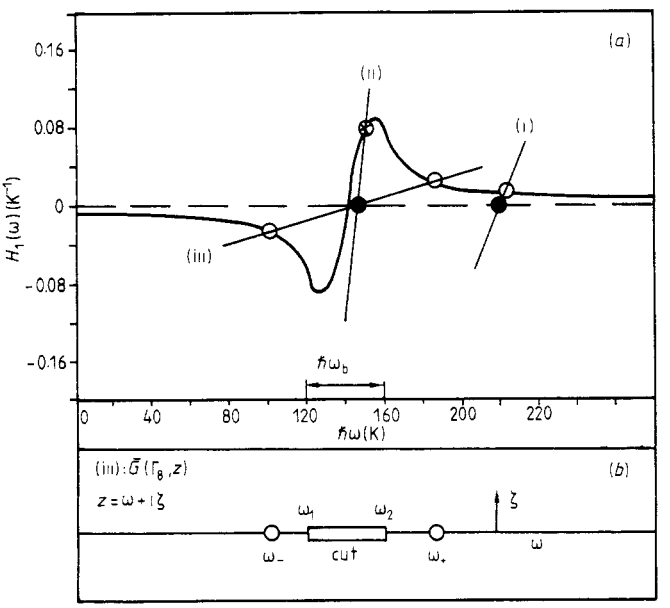

Figure 5. (*a*) Graphic solution of equation (30). The straight lines correspond to the LHS of (30) for different Δ, α. (i), non-resonant renormalistion of Δ to Δ'; (ii), Δ inside $[\omega_1, \omega_2]$ and weak coupling α: broadening into a lorentzian; (iii), strong coupling case: bound- and anti-bound-state solutions occur outside the phonon continuum $[\omega_1, \omega_2]$. ●, position of bare Δ; ○, poles of $\tilde{G}(\Gamma_8, \omega)$; ⊗, position of lorentz. (*b*) Analytic structure of $\tilde{G}(\Gamma_8, z)$ for case (iii).

(iii) If α^2 is sufficiently large, two solutions $\Delta_\pm$ exist far below Δ (and ω_1) and far above Δ (and ω_2), i.e. outside the phonon continuum. These solutions correspond to a bound state (Δ_-) and an anti-bound state (Δ_+) of a Γ_8 excitation and the phonons in the band $\omega_1 < \omega < \omega_2$. Irrespective of whether Δ was inside or outside $[\omega_1, \omega_2]$, $\Delta_\pm$ correspond to δ-function contributions to $S_c(\Gamma_8, \omega)$, i.e. poles of $\tilde{G}(\Gamma_8, \omega)$ lying on the real axis which do not have an intrinsic linewidth.

For the latter case the analytic structure of $\tilde{G}(\Gamma_8, z)$ in the complex z plane is indicated in figure 5(b). It is interesting to investigate how much weight is concentrated in the bound- and anti-bound-state poles of $\tilde{G}(\Gamma_8, \omega)$. Their contribution to $\tilde{G}$ is given by

$$G_b(\Gamma_8, \omega) = \frac{Z_-}{\omega - \Delta_- + i\eta} + \frac{Z_+}{\omega - \Delta_+ + i\eta} \tag{31}$$

where $Z_\pm = |1 - \alpha^2 H_1'(\Delta_\pm)|^{-1}$ with $H_1'(\omega) = \mathrm{d}H_1(\omega)/\mathrm{d}\omega$ are the weights of the poles at $\Delta_\pm$. From (23) one obtains

$$H_1'(\omega) = -\left(\frac{2}{\omega_b}\right)^2 \left(\ln\left|\frac{\omega - \omega_0}{\omega - \omega_1}\right| + \ln\left|\frac{\omega - \omega_0}{\omega - \omega_2}\right|\right). \tag{32}$$

In the symmetric case ($\Delta = \hbar\omega_0$) $Z_+ \equiv Z_-$. The variation of $Z_\pm$ with coupling strength g_0 is shown in figure 6(b) for two cases. The inequality $Z_+ + Z_- \leqslant 1$ is always fulfilled because the spectral function $S_c(\Gamma_8, \omega)$ is normalised to one. The quantity $1 - (Z_+ + Z_-)$ is the spectral weight of the cut; i.e.

$$1 - (Z_+ + Z_-) = \int_{\omega_1}^{\omega_2} S_c(\Gamma_8, \omega)\, \mathrm{d}\omega. \tag{33}$$

If Δ is inside $[\omega_1, \omega_2]$ and α becomes small then at a critical size α_c, the $\Delta_\pm$ poles merge into the phonon continuum while $Z_\pm \to 0$ for $\alpha \geqslant \alpha_c$. For $\alpha < \alpha_c$ all the spectral weight is concentrated in the cut interval $[\omega_1, \omega_2]$. If Δ were outside $[\omega_1, \omega_2]$ (say above ω_2) then for $\alpha \to \alpha_c$ the bound state at Δ_- merges into the continuum with $Z \to 0$ and the anti-bound state approaches the energy Δ' of the renormalised Γ_8 level.

It is easy to calculate the threshold value α_c from (30) and by inspection of figure 5(a) when at least one of the bound states vanishes. The condition is

$$\alpha_c = g_0^c \gamma_0 = \lambda\omega_b(1 + 2|x|)^{1/2}$$
$$\lambda = \tfrac{1}{2}(2\ln 2)^{-1/2} \qquad x = (\omega_0 - \Delta)/\omega_b \qquad \gamma_0 = (40)^{1/2} = 6.3. \tag{34}$$

The critical coupling constant $g_0^c(\Delta)$ is shown in figure 6(a). The shaded area corresponds to parameter pairs (Δ, g_0) which are compatible with bound-state energies and weights of $CeAl_2$. Clearly this compound is far into the bound-state region. This figure shows that even without extrinsic broadening by conduction electrons the bound states can only be observed if the magnetoelastic coupling g_0 is larger than a certain threshold value g_0^c. At this point it is useful to consider the dispersionless model as the limit $\hbar\omega_b \to 0$ of the present model. In this case

$$H_1(\omega) = \mathrm{P}\int \frac{D(\omega')}{\omega - \omega'}\,\mathrm{d}\omega' \simeq \frac{1}{\omega - \omega_0} \tag{35}$$

and (30) reduces to

$$(\omega - \omega_0)(\omega - \Delta) = g_0^2\gamma_0^2 \tag{36}$$

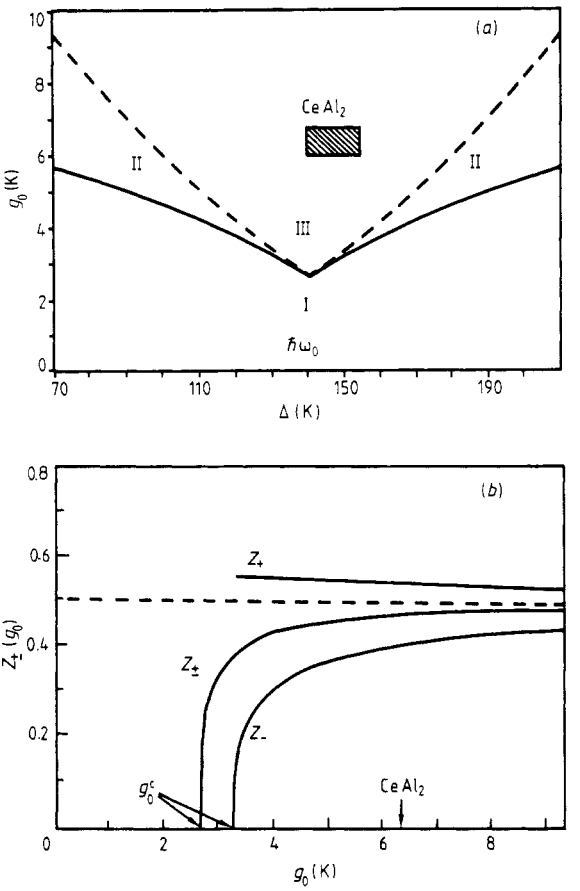

Figure 6. (*a*) Existence criterion for bound states as a function of (g_0, Δ). I, no bound states; II, bound states exist; but $R = \min(Z_+, Z_-)/\max(Z_+, Z_-) < 0.3$; III, bound states exist and $R > 0.3$. The full curve gives the threshold value $g_0^c(\Delta)$. The shaded area is compatible with the situation in $CeAl_2$. (*b*) Weight of bound-state poles as a function of coupling strength. Middle curve, $Z_+ = Z_-$ for $\Delta = 140$ K ($=\hbar\omega_0$); in this case $Z_\pm \to 0.5$ for large g_0. Upper and lower curves correspond to $\Delta = 150$; $Z_+ + Z_- < 1$ always.

whose solutions are identical to those in equation (7). Therefore the (anti-) bound-state poles correspond to the $\tilde{\Gamma}_{81}$ and $\tilde{\Gamma}_{82}$ states of the dispersionless model. Furthermore $Z_\pm = |1 + \alpha^2/(\Delta_\pm - \omega_0)^2| \to \frac{1}{2}$ for $\hbar\omega_b \to 0$ and $\Delta = \hbar\omega_0$. According to (33) no spectral contribution to $S_c(\Gamma_8, \omega)$ from the cut is left. This agrees with the fact that the $\tilde{\Gamma}_6$ state in the dispersionless model has no electronic component.

3.3.2. The magnetic cross section and the problem of vertex corrections. Until now it has been assumed that the bound-state poles of the CEF pseudo-fermion Green function $\tilde{G}(i, \omega)$ directly show up in the magnetic scattering cross section. The reason for this has to be investigated closer. According to (9) the dynamical susceptibility $u(\omega)$ is the quantity of interest. It can be calculated by simply replacing $\tilde{G}_0(i, \omega)$ with the renormalised $\tilde{G}(i, \omega)$ in the diagram for the susceptibility. This diagram is shown in figure 7(*a*) where the vertex operator $V = J_z$ is used. This leads to

$$u(\omega_n) = -\beta^{-1} \sum_{ij} |M_{ij}|^2 \sum_{\omega_{n'}} G(j, \omega_{n'}) G(i, \omega_n + \omega_{n'}). \tag{37}$$

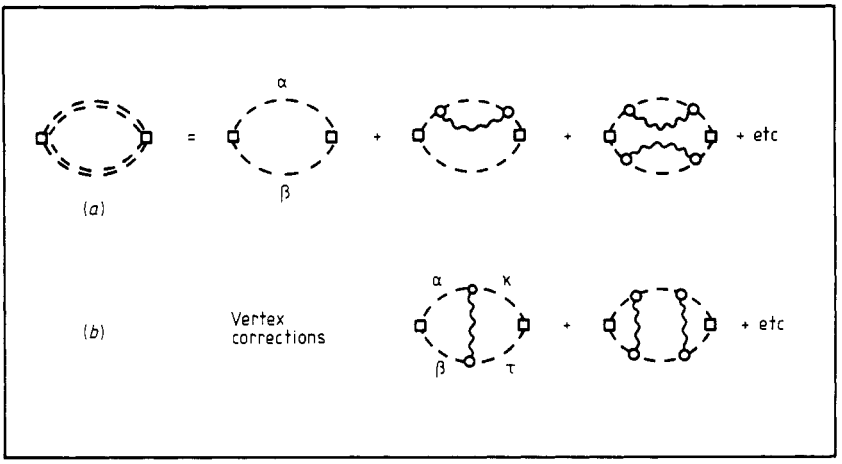

Figure 7. (*a*) Diagrammatic representation for the single-ion susceptibility corresponding to (37). First diagram on the rhs represents PPA expression for the dipolar ($V = J_z$) or quadrupolar ($V = O_\mu$) susceptibility. ($\square = V$). (*b*) Vertex corrections to the susceptibility. The open circles represent H_1.

Here $M_{ij} = \langle i|J_z|j\rangle$ and the proper limit $\lim_{\lambda\to\infty} \exp(-\beta\lambda)Z_0^{-1}$ has been assumed. Because the renormalised Green function (16) with $i = \Gamma_8$ has a cut along the real axis in the interval $[\lambda + \omega_1, \lambda + \omega_2]$, the summation over $\omega_{n'}$ in (37) is very difficult to perform in general. Therefore the cut contributions are neglected for simplicity, i.e. the approximate Green functions (29*a*) and (31) are used which have poles only. This leads to ($i\omega_n \to \omega + i\eta$)

$$u(\omega) = \sum_{\lambda\lambda'} |\tilde{M}_{\lambda\lambda'}|^2 \frac{p_\lambda - p_{\lambda'}}{\omega + \Delta_{\lambda'\lambda} + i\eta}. \tag{38}$$

Here $\Delta_{\lambda'\lambda} = \varepsilon_{\lambda'} - \varepsilon_\lambda$ and $p_\lambda = Z_0^{-1}\exp(-\beta\varepsilon_\lambda)$ (Z_0 is the partition function), $\varepsilon_\lambda = 0$, Δ_+ and Δ_- are the pole positions of $\tilde{G}(\Gamma_7, \omega)$ and $\tilde{G}_b(\Gamma_8, \omega)$, and p_λ is the corresponding thermal occupation. Furthermore, the matrix elements $|M'_{\lambda\lambda}|^2$ are given by the original CEF matrix elements, multiplied by Z_+ and Z_-, the weight of the (anti-) bound-state poles if λ, $\lambda' = \Gamma_{8-}(\Delta_+), \Gamma_{8-}(\Delta_-)$.

For example

$$|\tilde{M}_{77}|^2 = |M_{77}|^2$$
$$|\tilde{M}_{78-}|^2 = Z_-|M_{78}|^2 \qquad |\tilde{M}_{78+}|^2 = Z_+|M_{78}|^2. \tag{39}$$

The magnetic cross section (9) is proportional to Im $u(\omega)$. According to (38) this leads to δ-peaks at the energies Δ_+, Δ_- whose weights are given by $|\tilde{M}_{78+}|^2$ and $|\tilde{M}_{78-}|^2$. In the limit $\hbar\omega_b \to 0$ one has $Z_+ + Z_- \to 1$. This agrees with the results of the dispersionless model of § 3.2. As long as $\hbar\omega_b$ is finite $Z_+ + Z_- < 1$ and the remaining intensity required to fulfil the sum rule is due to the cut contribution to $u(\omega)$. This would be a smooth function of ω restricted to the interval $[\omega_1, \omega_2]$. Additional inclusion of broadening due to exchange interaction as in the dispersionless model could in principle also be done within the present Green function formalism along the lines given by Fulde and Peschel (1972). However, the main purpose here was to demonstrate that the bound-state poles of $G(\Gamma_8, \omega)$ show up directly in the magnetic cross section if the LHS of figure 7(*a*) is the correct diagrammatic represen-

tation for $u(\omega)$. That this is so can be justified by considering the influence of vertex corrections: as shown in figure 7(a), equation (37) means a summation of an infinite series of diagrams of a particular type. This series produces the characteristic bound-state contributions in Im $u(\omega)$ only if vertex correction diagrams such as those shown in figure 7(b) can be neglected. The first vertex correction in figure 7(b) is given by

$$V_1(\omega) = \sum_{\alpha\beta,\kappa\tau} \Gamma^{\alpha\beta}_{\kappa\tau} F_{\alpha\beta,\kappa\tau}(\omega)$$

$$\Gamma^{\alpha\beta}_{\kappa\tau} = \sum_{\mu} \sum_{rs,nm} \langle \beta s|V|\alpha r\rangle \langle \alpha r|O_\mu|\kappa n\rangle \langle \kappa n|V|\tau m\rangle \langle \tau m|O_\mu|\beta s\rangle. \tag{40}$$

$F_{\alpha\beta,\kappa\tau}(\omega)$ is a complicated function whose ω dependence is not of interest here. Again $\alpha\beta\kappa\tau$ denote the CEF multiplets, RSNM are degeneracy indices and $\mu = 1, 2, 3$. For the dipolar vertex $V = J_z$ the summation leads to the result

$$\Gamma^{\alpha\beta}_{\kappa\tau} = \begin{cases} 0\,(\alpha\beta) & \text{and } (\kappa\tau) \neq (\Gamma_8\Gamma_8) \\ \neq 0\,(\alpha\beta) & \text{or } \quad (\kappa\tau) = (\Gamma_8\Gamma_8). \end{cases} \tag{41}$$

This shows that vertex corrections to the diagrams with $(\alpha\beta) = (\Gamma_7\Gamma_8)$ in figure 7(a) are identical to zero and therefore the summation leading to the LHS of figure 7(a) is justified. The vertex corrections for $(\alpha\beta) = (\Gamma_8\Gamma_8)$ in figure 7(a) are non-zero but they influence Im $u(\omega)$ only for $\omega \simeq 0$ and not in the bound-state region.

3.4. Temperature dependence of the renormalised phonons

Until now only the magnetic scattering cross section has been considered. As mentioned in the beginning however, at large momentum transfer the phonon scattering cross section dominates. In this way the phonon branches of $CeAl_2$ could be determined in great detail at room temperature (296 K) (Reichardt 1983). At lower temperatures (77 K, 4 K) some typical branches have also been measured and it was found that they show a pronounced softening over the whole Brillouin zone (Reichardt 1983). Because this softening is absent in $LaAl_2$ its origin in $CeAl_2$ must again lie in the magnetoelastic coupling to the 4f states. The phonon scattering cross section can be related to the phonon Green function $D(\boldsymbol{k}s, \omega)$ by using the FDT theorem and equation (1):

$$\left(\frac{d^2\sigma}{d\omega\, d\Omega}\right)_{\text{phon.}} \sim [1 - \exp(-\beta\omega)]\, \text{Im}\, D(\boldsymbol{k}s, \omega). \tag{42}$$

Here polarisation factors and the form factor have been suppressed. The Dyson equation for the renormalised $D(\boldsymbol{k}s, \omega)$ is expressed by figure 4(b) in the RPA. It leads to

$$D(\boldsymbol{k}s, \omega)^{-1} = D_0(\boldsymbol{k}s, \omega)^{-1} - \Sigma_Q(\boldsymbol{k}s, \omega)$$

$$\Sigma_Q(\boldsymbol{k}s, \omega) = \sum_{\mu} |g^{\mu}_{\boldsymbol{k}s}|^2\, u_Q(\omega). \tag{43}$$

The quadrupolar self-energy Σ_Q is determined by the quadrupolar single-ion susceptibility u_Q which in the RPA is equivalent to the 'bubble' diagram figure 4(b). Explicitly the RPA expression is

$$u_Q(\omega) = \sum_{ij} O^{\mu}_{ij} O^{\mu}_{ji} \frac{p_i - p_j}{\omega + \Delta_{ji} + i\eta} \qquad O^{\mu}_{ij} = \langle i|O_\mu|j\rangle. \tag{44}$$

This in independent of μ due to the cubic symmetry. $\Delta_{ji} = \varepsilon_j - \varepsilon_i$; ε_i are the unperturbed

CEF excitation energies and p_i their thermal occupations. One might question whether the RPA is sufficient for the quadrupolar susceptibility because in the expressions for the dipolar susceptibility, (37) and (38), the renormalised Green functions $\tilde{G}(i, \omega)$ were used for the calculation of the susceptibility 'bubble' of figure 7(a). However, this was only reasonable because the vertex corrections in figure 7(*b*) could be neglected. For the quadrupolar susceptibility this is not possible. Using the quadrupolar vertex $V = O_\mu$ ($\mu = 1, 2, 3$) in figure 7 and equation (40) one finds $\Gamma^{\alpha\beta}_{\kappa\tau} \neq 0$ for $(\alpha\beta) = (\kappa\tau) = (78)$, (87). Therefore the contributions in figure 7(*a*) with $(\alpha\beta) = (78)$, (87) have strong vertex corrections of the type shown in Fig. 7(*b*). Because $u_Q(\omega)$ cannot be expressed directly by $\tilde{G}(i, \omega)$ as in figure 7(*a*), it will not have a double-peak structure due to (anti-) bound states as did the dipolar $u(\omega)$. Instead, it is reasonable to assume that the proper $u_Q(\omega)$ will have a similar structure as the RPA expression with a single peak at Δ which, however, should be strongly broadened due to the higher-order processes in figure 7. This will be simulated by a temperature-independent linewidth Γ for the Γ_7–Γ_8 transition at Δ, i.e. the replacement $\Delta \rightarrow \Delta + i\Gamma$ is made in (44). Because the functional dependence of g^μ_{ks} on ks is not known $g^\mu_{ks} \equiv g_0$ is assumed and therefore only the temperature dependence of the average phonon energy $\hbar\omega_{av}$ can be calculated from (43) and (44). At high temperatures $kT \gg \Delta\hbar\omega_{av} \equiv \hbar\omega_0$, the centre of the unrenormalised PDOS. For the phonon spectral function one obtains:

$$S_{ph}(\omega) = [1 - \exp(-\beta\omega)]^{-1} \operatorname{Im} D(\omega) = \frac{4\omega_0^2[1 - \exp(-\beta\omega)]^{-1}\Sigma_2(\omega)}{(\omega_0^2 - \omega^2 - 2\omega_0\Sigma_1(\omega))^2 + 4\omega_0^2\Sigma_2(\omega)^2} \tag{45}$$

where according to (43) and (44) the real and imaginary parts of Σ are given by

$$\Sigma_1(\omega) = -\alpha^2 f(T)\frac{(\omega^2 - \Delta^2 - \Gamma^2)/2\omega_0}{(\omega^2 + \Delta^2 + \Gamma^2)^2 - 4\omega^2\Delta^2}$$

and

$$\Sigma_2(\omega) = \alpha^2 f(T)\frac{(\omega/\omega_0)\Gamma}{(\omega^2 + \Delta^2 + \Gamma^2)^2 - 4\omega^2\Delta^2} \tag{46}$$

with

$$\alpha^2 = 4\Delta\omega_0 g_0^2 Q_{78} \qquad Q_{78} = \sum_{mn} |\langle\Gamma_7^n|O_\mu|\Gamma_8^m\rangle|^2 = 53.3$$

and

$$f(T) = p_7 - p_8 = \tfrac{1}{2}[1 - \exp(-\beta\Delta)]/[1 + 2\exp(\beta\Delta)].$$

The coupling constant $g_0 = 6.3$ K is the same as has been determined before from the magnetic structure function. The Γ_7–Γ_8 linewidth Γ is the only adjustable parameter. Figure 8 shows a plot of $D_2(\omega) = \operatorname{Im} D(\omega)$ for several temperatures. The average phonon frequency $\hbar\omega_{av}$ has to be interpreted as the peak of $S_{ph}(\omega)$. At room temperature $\hbar\omega_{av}$ is almost the same as $\hbar\omega_0$ because then $f(T)$ and therefore $\Sigma_1(\omega)$ is already quite small. Lowering the temperature leads to a strong reduction in $\hbar\omega_{av}$ because of the increasing magnetoelastic self-energy. In figure 8(*b*) the renormalised phonon frequency $\hbar\omega_{av}$ is plotted as a function of temperature for $\Gamma = 25$ K. The experimental values (Reichardt 1983) at $T = 296$, 77 and 4 K are indicated for comparison. These values are uncertain by about ± 5 K because it is not easy to extract a proper average value $\hbar\omega_{av}$ from the measured branches. However, the general agreement is quite reasonable. The calculated

$\hbar\omega_{av}$ does not depend dramatically on the phenomenological linewidth Γ. For comparison the case $\Gamma = 0$ which corresponds to the RPA for $u_Q(\omega)$ (44) is also shown. In this approximation $\hbar\omega_{av}$ corresponds directly to one of the poles of $D(\omega)$ in (43). There is an additional pole present originating from the CEF excitation at Δ, whose weight is strongly suppressed by a finite Γ. Its remnant can still be seen in figure 8(*a*) as a small hump at

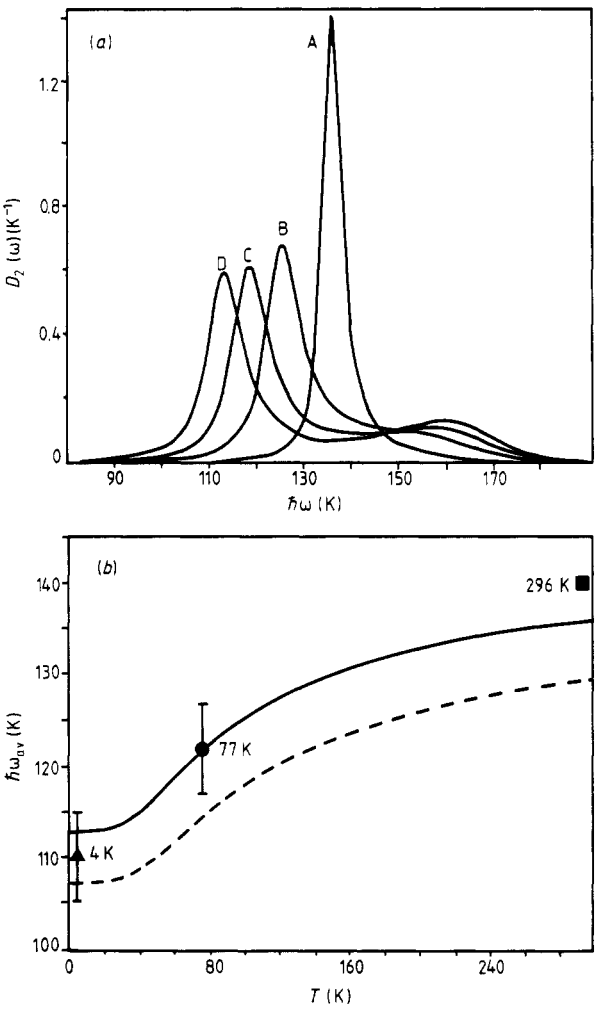

Figure 8. (*a*) Spectral function of renormalised phonons for several temperatures: A, 300 K; B, 100 K; C, 60 K; D, 10 K. Here values of $\Delta = 150$ K and linewidth $\Gamma = 25$ K have been chosen. (*b*) Temperature dependence of the average phonon frequency $\hbar\omega_{av}$ for $\Gamma = 0$ = RPA (broken curve) and $\Gamma = 25$ K (full curve). Squares are from experimental results of Reichardt (1983).

$\hbar\omega \simeq 170$ K which is probably smaller than the experimental background. One also observes from figure 8(*a*) a broadening of the phonon spectral function when T decreases. This has actually been observed. To describe this effect properly, however, a better theory for $u_Q(\omega)$ without a phenomenological Γ would be necessary.

4. Influence of the CEF–phonon bound state on the thermodynamic properties of $CeAl_2$

It is well known that CEF states have a pronounced effect on thermodynamic properties because their energies are of the order $\leqslant 100$ K and can therefore be thermally populated. The most common quantities which show a strong T-dependence in the range of the CEF energies are the specific heat C_m (Schottky anomalies), the magnetic susceptibility χ_m and the thermal expansion coefficient β. A review of the theory and some experimental examples for these quantities in conventional CEF systems have been given by Fulde (1978) and Lüthi (1980). It is quite simple to calculate C_m, χ_m and β for a normal Γ_7–Γ_8 CEF system. In this chapter I want to discuss the qualitative influence of the existence of bound states in $CeAl_2$ on these quantities. A quantitative discussion is difficult because of Kondo-type anomalies and cooperative magnetic effects in $CeAl_2$ (Steglich *et al* 1979). The thermodynamic quantities will be calculated within a single-ion approximation (no cooperative effects) using the dispersionless model for the bound states.

4.1. Specific heat

In a conventional CEF system the Schottky contribution to C_m is given by $-T^{-1}(\partial^2 F_m/\partial T^2)$ where F_m is the free energy due to CEF excitations. This leads to the following molar specific heat (R is the gas constant) (Lüthi 1980):

$$C_m/R = (\langle \varepsilon^2 \rangle - \langle \varepsilon \rangle^2)/(kT)^2. \tag{47}$$

Here $\langle A \rangle = Z^{-1} \sum_i A_i \exp(-\varepsilon_i/kT)$ is the thermal average. This formula can also be used if CEF–phonon bound states are present, provided the thermal average is redefined as

$$\langle \tilde{A} \rangle = \tilde{Z}^{-1} \sum_i A_i \exp(-\varepsilon_i/kT) \qquad \text{where } i = \{|\tilde{\Gamma}^n_\alpha\rangle, i = 1, \ldots, 24\}$$

are the eigenstates of the coupled CEF–phonon system starting from a decoupled system that includes all the zero- and one-phonon states. The partition function is given by $\tilde{Z} = \sum_i \exp(-\tilde{\varepsilon}_i/kT)$. This has to be done in order to ensure factorisation $\tilde{Z} = Z_{ph}Z$ into phonon and CEF partition functions in the limit $g_0 \to 0$. A reasonable approximation is to use the $\tilde{\varepsilon}_i$ of § 3.2 for $i = 1, \ldots, 12$ and the undisturbed $\tilde{\varepsilon}_i = \Delta + \hbar\omega_0$ for $i = 13, \ldots, 24$. The specific heat $\tilde{C}_m$ calculated with (47) by using $\langle \tilde{A} \rangle$ contains all the contributions of one-phonon excitations. These have to be subtracted in order to obtain the explicit expression for C_m which corresponds to the CEF contribution modified by the existence of bound states

$$C_m/R = \tilde{C}_m/R - 3x^2 \exp(x)/[3 + \exp(x)]^2 \qquad x = \hbar\omega_0/kT. \tag{48}$$

Because $\hbar\omega_0$ is the temperature-independent bare-phonon frequency, (48) should be associated with the experimental difference $C_m^{exp} = C_m^{tot}(CeAl_2) - C_m^{tot}(LaAl_2)$ where C_m^{tot} is the total molar specific heat. This is not really the Schottky contribution in $CeAl_2$ because the phonon frequencies for $CeAl_2$ are themselves temperature dependent. In the limit $g_0 \to 0$, (48) reduces to (47).

A plot of C_m for a conventional Γ_7–Γ_8 system and for the bound-state system is shown in figure 9. One can see that the Schottky peak of the Γ_7–Γ_8 system is broadened due to the presence of two inelastic excitations in the system with bound states. A comparison with experiment is difficult because C_m^{exp} has not been measured accurately (Deenadas

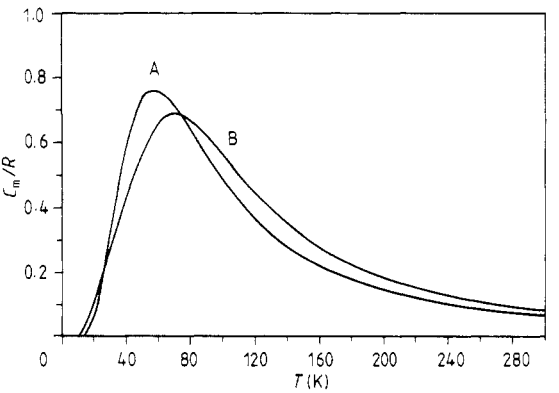

Figure 9. The CEF contribution to the molar specific heat C_m. (R is the gas constant). A. Conventional Γ_7–Γ_8 system; B. system with bound states according to figure 3 with Δ = 150 K.

et al 1970); it is very small compared with C_m^{tot}. Better measurements are now being performed (Schefzyk *et al* 1983). One should not expect quantitative agreement with (48) because the phonons have been treated in a very simple model. One would expect that (48) is not good for $kT \ll \hbar\omega_0$ and $kT \geq \hbar\omega_0$. However the basic feature of a broadened Γ_7–Γ_8 Schottky peak due to the splitting between (anti-) bound states should be observable.

4.2. *Magnetic susceptibility*

The magnetic susceptibility can be calculated by a similar generalisation from the conventional CEF expression for χ_m (Fulde 1978). The details will not be given here because the result is not very significant. The inclusion of bound-state effects changes χ_m only within 2% compared with a normal Γ_7–Γ_8 system. Recent susceptibility measurements (Aarts *et al* 1983) show that for $T \geq 50$ K the experimental slope of $\chi_m^{-1}(T)$ is smaller by about 20% compared with the prediction of a single-ion susceptibility calculation. The origin of this discrepancy is not known at present.

4.3. *Thermal expansion*

In materials without magnetic ions the thermal expansion coefficient $\beta = V^{-1}(\partial V/\partial T)_p$ is determined by the anharmonic part of the lattice potential. If ions with CEF states are present an additional, at low temperatures much stronger contribution exists which is caused by the fully symmetric magnetoelastic interaction. It is given by Lüthi (1980)

$$\beta = \kappa R(\langle\varepsilon^2\gamma\rangle - \langle\varepsilon\rangle\langle\gamma\rangle)/(kT)^2 \tag{49}$$

(κ is the compressibility). Here $\gamma_i = -\partial \ln \varepsilon_i/\partial \ln V$ is the 'Grüneisen parameter' of the CEF level ε_i. This formula is quite similar to (47) for C_m. In fact, for a conventional two-level system, e.g. Γ_7, Γ_8; $\langle\varepsilon^2\gamma\rangle = \gamma_0\langle\varepsilon^2\rangle$ and $\langle\varepsilon\gamma\rangle = \gamma_0\langle\varepsilon\rangle$ where γ_0 corresponds to the upper (Γ_8) level. This leads to $\beta \sim C_m$; i.e. they should have the same T dependence. Now in $CeAl_2$ the Γ_8 level is split into bound states whose 'Grüneisen parameters' $\gamma_\pm$ will be different from each other, therefore $\beta \sim C_m$ cannot be expected to hold for $CeAl_2$. Using (7) $\gamma_\pm$ can be calculated under the assumption that $\partial(\hbar\omega_0)/\partial V = 0$, i.e. the lattice

Grüneisen parameter is zero. This leads to

$$\gamma_{\pm} = \gamma_0 f_{\pm}(x) \qquad f_{\pm}(x) = \tfrac{1}{2}x\,\frac{1 \mp (1-x)^{-1}D(x)}{(1-x)/2 \pm D(x)}$$

$$D(x) = [\tfrac{1}{4}(1-x)^2 + g_0^2\gamma_0^2/\hbar\omega_0] \qquad x = \hbar\omega_0/\Delta. \tag{50}$$

Here $\gamma_0 = -(\partial \ln \Delta/\partial \ln V)$ is the Grüneisen parameter of the original CEF gap. Using (49), $\beta(T)$ is calculated and the ratio $\beta(T)/C_m(T)$ is plotted in figure 10. As mentioned this is expected to be a constant for a true two-level system. However, a strong variation of this ratio below 100 K is predicted for $CeAl_2$. Experimentally this has not yet been tested. Experiments which are under way (Schefzyk *et al* 1983) should be able to test this prediction, although the situation is complicated by Kondo contributions at low temperatures.

5. Summary

It has been demonstrated that the magnetoelastic interaction of phonons and 4f states is responsible for the previously unexplained magnetic excitation spectrum which has been observed in $CeAl_2$ and its alloys with La and Sc. This interaction leads to bound- and anti-bound states below and above the region of maximum phonon density of states. The intensity sum rule can be explained naturally by this model. The coupling strength as determined from bound-state splitting agrees reasonably well with results from elastic constant measurements. In all the other MAl_2 (M = RE) the existence of the bound state is less likely because the coupling constants are generally smaller. Within the dispersionless model the qualitative features of the magnetic structure function could be explained by assuming an exchange interaction with conduction electrons. In addition, the magnetoelastic coupling leads to a strong temperature-dependent renormalisation of the phonons which can be adequately described by a quadrupolar response function.

The existence of bound states should also influence thermodynamic properties, notably the specific heat where one would expect a broadening of the Schottky peak. Furthermore, the ratio of thermal expansion and specific heat should be strongly temperature dependent instead of being a constant as for a conventional two-level CEF system.

One could imagine several improvements and extensions of the theory presented here. The properties of phonons and their coupling to 4f states have been treated in a rather simple way in which only the PDOS and a single coupling constant enters. A more detailed calculation which incorporates the wavevector and polarisation dependence of phonon frequencies and coupling parameters would be desirable. The quadrupolar response function which leads to the phonon temperature dependence should be calculated in a better approximation. The consequences of bound states for transport properties, resistivity and thermopower etc should also be investigated, especially because $Ce_xLa_{1-x}Al_2$ is usually taken as a model Kondo system where only conventional Γ_7–Γ_8 states are used.

It will be interesting to look for CEF–phonon bound states in other compounds. Ce compounds are the most likely candidates due to the unusually strong lattice interaction of the Ce^{3+}–4f states. Recent Raman scattering experiments (Schaack *et al* 1983) indicate that these states may also have been observed in CeF_3. It is possible that similar states also exist in 3d compounds (Wagner and Koidl 1980). In $CeAl_2$ it would be interesting

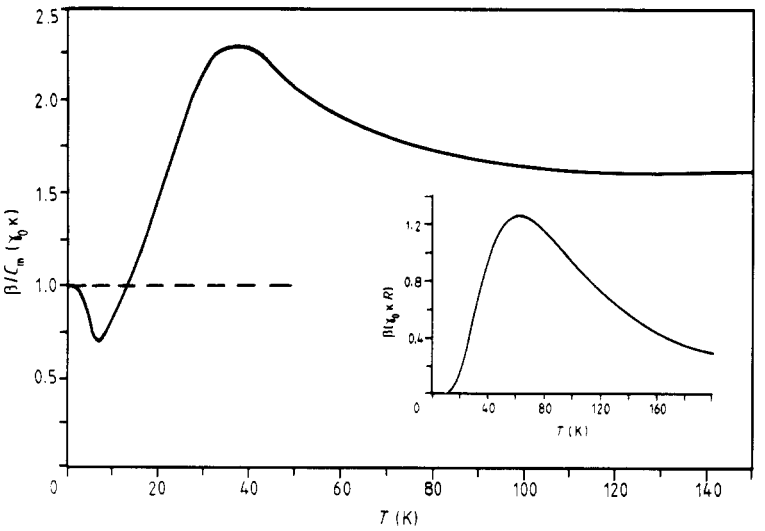

Figure 10. Inset: thermal expansion β as function of T. (κ is the compressibility; γ_0 is the 'Grüneisen constant', R is the gas constant). The ratio of β/C_m is plotted for the level system with $\tilde{\Gamma}_{8(1,2)}$ bound states. For a conventional $\Gamma_7\Gamma_8$ system β/C_m would be independent of T (broken line).

to investigate the effects of an external magnetic field on the bound states and the phonon temperature anomalies. Spin-polarised neutron scattering would probably be very helpful for further investigations on $CeAl_2$ but unfortunately this is experimentally not possible at present.

Acknowledgment

The author would like to express many thanks to Dr Reichardt for making his experimental results available before publication. Helpful and stimulating discussions with Professor P Fulde are also gratefully acknowledged.

References

Aarts J 1983 to be published
Ahrens K 1980 *Z. Phys.* B **26** 49–58
Barbara B, Rossignol M F, Boucherle J X, Schweitzer J and Buevoz J L 1979 *J. Appl. Phys.* **50** 2300–7
Bauer E, Gratz E, Mikovits W, Sassik H and Kirchmayr H 1982 *J. Magn. Magn. Mater.* **29** 192–6
Becker K W, Fulde P and Keller J 1977 *Z. Phys.* B **28** 9–18
Cullen J R and Clark A E 1977 *Phys. Rev.* B **15** 4510–5
Deenadas C, Thompson A W, Craig R S and Wallace W E 1970 *J. Phys. Chem. Solids* **32** 1853–66
Fulde P 1978 *Handbook on the Physics and Chemistry of Rare Earths* vol 2, eds K A Gschneidner and L Eyring (Amsterdam: North-Holland) pp 295–386
Fulde P and Peschel I 1972 *Adv. Phys.* **21** 1–67
Gehring G A and Gehring K A 1975 *Rep. Prog. Phys.* **38** 1–89
Godet M and Purwins H G 1977 *Solid State Commun.* **21** 761–3
Horn S 1983 to be published
Jullien R, Pfeuty P, Fields J N and Doniach S 1979 *J. Physique Coll.* **40** C5 293–300

Lax M 1974 *Symmetry Principles in Solid State and Molecular Physics* (New York: Wiley)
Lingner C and Lüthi B 1983 *J. Magn. Magn. Mater.* **36** 86
Loewenhaupt M, Rainford B D and Steglich F 1979 *Phys. Rev. Lett.* **25** 1709–12
Lüthi B 1980 *Dynamical Properties of Solids* vol 3, eds G K Horton and A A Maradudin (Amsterdam: North-Holland) pp 245–92
Lüthi B and Lingner C 1979 *Z. Phys.* B **34** 157–63
Maple M B 1976 *Appl. Phys.* **9** 179–204
Parks R D, Kupferberg L C, Croft M C, Shapiro S M and Gurewitz E 1979 *J. Physique Coll.* **40** C5 323–5
Penney T, Barbara B, Plaskett T S, King H E Jr and LaPlaca S J 1982 *Solid State Commun.* **44** 1199–204
Reichardt W 1983 to be published
Schaak G 1977 *Z. Phys.* B **26** 49–58
Schaak G *et al* 1983 to be published
Schefzyk R *et al* 1984 to be published
Steglich F, Bredl C D, Loewenhaupt M and Schotte K D 1979 *J. Physique Coll.* C5 Suppl. 301–7
Thalmeier P and Fulde P 1982 *Phys. Rev. Lett.* **49** 1588–91
Toyozawa Y and Hermanson J 1968 *Phys. Rev. Lett.* **21** 1637–41
Wagner V and Koidl P 1980 *J. Magn. Magn. Mater.* **15–18** 33–34